

# A potential new method for determining the temperature of cool stars

S. Viti<sup>1</sup>, H. R. A. Jones<sup>2</sup>, M. J. Richter<sup>3</sup>, R. J. Barber<sup>1</sup>, J. Tennyson<sup>1</sup>, J. H. Lacy<sup>4</sup>

<sup>1</sup>*Dept. Physics and Astronomy, University College London, Gower Street, London, WC1E 6BT, UK*

<sup>2</sup>*Centre for Astrophysics Research, University of Hertfordshire, College Lane, Hatfield, Hertfordshire AL10 9AB, UK*

<sup>3</sup>*Physics Department, UC Davis, One Shields Ave, Davis, CA 95616, USA*

<sup>4</sup>*Department of Astronomy, University of Texas at Austin, 1 University Station, Austin, TX 78712, USA*

Released 2002 Xxxxx XX

## ABSTRACT

We present high resolution ( $R = 90,000$ ) mid-infrared spectra of M dwarfs. The mid infrared region of the spectra of cool low mass stars contain pure rotational water vapour transitions that may provide us with a new methodology in the determination of the effective temperatures for low mass stars. We identify and assign water transitions in these spectra and determine how sensitive each pure rotational water transition is to small (25 K) changes in effective temperature. We find that, of the 36 confirmed and assigned pure rotational water transitions, at least 10 should be sensitive enough to be used as temperature indicators.

**Key words:** Stars: low mass - stars: atmospheres - stars: fundamental parameters - infrared: stars

## 1 INTRODUCTION

Low mass stars (LMS) constitute  $\sim 80\%$  of our stellar neighbourhood. They provide a probe of our understanding of main sequence stellar evolution and are key in determining the boundary between stellar and sub stellar objects. However, their spectra are extremely rich in structure and their opacity is made up of many molecular and atomic absorbers, each with hundred of thousands to millions of spectral lines. This means that colours are not easily interpretable as diagnostic of their properties. Among the fundamental properties of LMS, of particular importance is their effective temperature,  $T_{eff}$ : the latter has frequently been investigated but it is still not well determined. In

particular there is not yet a tight correlation between spectral type and effective temperature as there has been a long standing discrepancy between empirical effective temperatures and those derived by synthetic spectra ( $\sim 125$  K as estimated by Kirkpatrick et al. 1993). This is primarily due to the lack of a complete inclusion of molecular and atomic opacities in the models, in particular in the near infrared (NIR). Modelling the atmosphere of LMS in the NIR is not a trivial task: water vapour dominates this part of the spectrum and at the effective temperature applicable to cool star atmospheres ( $<4000$  K) water can access energies as high as  $45000\text{ cm}^{-1}$  before it dissociates; to reproduce high temperature water spectra is very challenging because of the complexity of the vibrational and rotational motion of asymmetric triatomic molecules. Leggett et al. (2000, 2001) used a synthetic grid which includes the water linelist calculated by Partridge & Schwenke (1997) to determine fundamental parameters for a large sample of LMS. They conclude that problems remain with the match of the observed water bands. Allard et al. (2000) also find that the models including this water linelist reproduce well late-type dwarfs but fail to reproduce hotter dwarfs. The main sources of error in present water opacity databases are the incorrect high temperature transitions (Jones et al. 2002, 2005).

Recently a new water linelist, BT2, has been produced (Barber et al. 2006). The BT2 linelist is by far the most complete linelist available, reaching higher energies than previously published. A comparison between a previous release of the BT2 linelist (BT1) and the PS linelist showed that at higher temperatures ( $T > 2000\text{K}$ ) the PS linelist is missing around 25 per cent of the water vapour opacity (Jones et al. 2005). While the BT2 increases the accuracy of the fitting in the NIR region, its cut off at energies above  $30000\text{ cm}^{-1}$  still means that none of the energy levels above  $20000\text{ cm}^{-1}$  are capable of being excited by  $1\text{ }\mu\text{m}$  photons (Barber et al. 2006).

Although the strongest water vapour opacity is at shorter wavelengths, analysis of sunspots (Wallace et al. 1995) shows that  $\text{H}_2\text{O}$  also accounts for the majority of lines in the mid infrared (MIR) region between  $8$  and  $21\text{ }\mu\text{m}$ . Polyansky et al (1997a,b) successfully assigned many of the water transitions in the 10-13 micron spectra of sunspots with further recent assignments being made in conjunction with the analysis of oxy-acetylene emission spectra (Coheur et al. 2005; Zobov et al. 2006). In this spectral region the water transitions are largely pure rotational, in contrast to the vibration-rotation transitions which dominate at shorter wavelengths. The use of pure rotational transitions greatly simplifies the spectral analysis as estimates of the transition strengths are much more straightforward. To a good approximation the strength of individual rotational transitions can be estimated from a simple algebraic formula times a Boltzmann factor. Furthermore, the presence of pure rotational transitions within different vibrational states, which is characteristic

of the sunspot spectrum, yields a large dynamic range for temperature analysis. These advantages potentially make the MIR region ideal for the determination of the effective temperature scale for LMS.

Here we propose a new methodology for establishing the effective temperatures of cool stars, in particular LMS, based on high resolution MIR spectroscopy. Taking advantage of the relatively easy to interpret MIR spectrum in cool stars has been done before: Ryde et al. (2006) used high resolution observations of water vapour in super-giants to show that classical photosphere models can not fit the observed spectra and that synthetic spectra based on cooler photospheric temperature structure are needed. This supports the idea that individual rotational water lines are highly sensitive to temperature variations in this region. In this paper we present the *first* high resolution (90,000) MIR observational data for two M dwarfs, together with one M giant. Our observations are described in Section 2. In Section 3 we present the data, the identification of the water lines and a theoretical sensitivity study using the BT2 linelist. In Section 4 we briefly conclude.

## 2 OBSERVATIONS

The data were taken in November 2006 using the Texas Echelon-cross-Echelle spectrograph (TEXES, Lacy et al. 2002) at the Gemini North 8m telescope. The observations were made on the nights of Nov 20, 23, and 27 for a total of  $\sim 13$  hours. We observed three objects (BS587, GJ411 and GJ273 - see Table 1) in the TEXES high spectral resolution mode in two grating positions: 11.2 and 12.5  $\mu\text{m}$  (800 and 892.857  $\text{cm}^{-1}$ ). The two grating positions were chosen on the basis of a relative lack of narrow telluric features and abundance of temperature sensitive water features based on an early version of our ab initio water line list, as well as of a careful analysis of the sunspot ( $T \sim 3300\text{K}$ ) 10-13  $\mu\text{m}$  spectrum. The spectral coverage was 0.5% at 11.2  $\mu\text{m}$  and 0.75% at 12.5  $\mu\text{m}$ . At 12.5  $\mu\text{m}$ , there are slight gaps in the spectral coverage because the angular width of the spectral orders is larger than the detector. The spectral resolution, as determined by Gaussian fits to telluric atmospheric lines in the 12.5  $\mu\text{m}$  setting, has a FWHM equivalent to  $R=90,000$ . We expect the same spectral resolution at 11.2  $\mu\text{m}$ . The slit width was 0.5'' for all observations and the length was roughly 4'' and 2.5'' at 11.2  $\mu\text{m}$  and 12.5  $\mu\text{m}$ , respectively. For all observations, we nodded the source along the slit roughly every 10 seconds.

Of our targets, GJ411 and BS587 were sufficiently bright to fine tune pointing based on the signal recorded from every nod pair. GJ273 was weaker and required accumulation of several nod pairs to evaluate pointing adjustments with confidence. On Nov 23, clouds were occasionally

**Table 1.** Properties of objects.

Object	RA	Dec	Sp.	d (pc)	$v_{rad}$ (km/s)	$M_{bol}$	$T_{eff}$ (K)	log g
GJ411 <sup>1</sup>	11 03 20.2	+35 58 11.5	M2V	2.52	-84.74	8.88	3510	5
BS587 <sup>2</sup>	02 00 26.8	-08 31 25.9	M4.6III	182	+12.70		3425	-1
GJ273 <sup>3</sup>	07:27:24.5	+05:13:32.5	M3.5V	3.76	+18.10	9.56	3150	5

<sup>1</sup> Effective temperature taken from Tsuji et al. (1996); surface gravity from Jones et al. (1996);  $M_{bol}$  from Cushing et al. (2005).

<sup>2</sup> Effective temperature taken from van Belle et al., (1999); surface gravity from Fluks et al., (1994).

<sup>3</sup> Effective temperature taken from Tsuji et al. (1996); surface gravity from Jones et al. (1996);  $M_{bol}$  from Delfosse et al. (1998).

present based on elevated background signal through TEXES. We discarded the data that were most severely effected.

Coordinates and properties of the three objects are listed in Table 1. The two dwarfs were chosen among a sample of well studied dwarfs: note that for both GJ411 and GJ273, the quoted temperatures have an uncertainties of at least 100K (cf Kirkpatrick et al 1993 and Tsuji et al. 1996). The quoted radial velocities are from the literature (Marcy et al. 1987) and they match the sunspot features within 0.5 km/s.

The data were reduced according to standard procedures as described in Lacy et al (2002). The TEXES pipeline provides for differencing of individual nod pairs, correcting spikes and cosmic rays, establishing a wavelength scale based on a user-identified telluric line, correcting distortions in the instrument, extracting 1D spectra using optimal weighting along the slit length, and combining spectra from the same night weighted by the square of their signal-to-noise ratio. The pipeline also performs flat-fielding and a first order correction for telluric spectral features using the difference between an ambient temperature blackbody and sky emission. Further flat-field and telluric correction comes from division by a featureless point source such as an asteroid or hot star. Data from separate nights were aligned spectrally and combined according to the square of their signal-to-noise ratio using custom IDL procedures. The dispersion calculations are accurate to 0.6 km/s or better.

### 3 ANALYSIS

Figures 1 and 2 show the recorded spectra for our sample for the two wavelength regions. The gaps in the spectra coincide with the removals of bad pixels and of telluric lines. The signal to noise varies from star to star ( $\sim 100$  for BS587, 40 for GJ411 and 5 for GJ273). We used the bright star BS587 as a template for the identification of the water lines in the spectra due to its high S/N. In total we identified 71 lines in the observed spectra which could potentially be water (see Table 2); however, only 52 of them are confirmed by comparison with the BT2 linelist (see Table 2 and Figures 3 and 4), some of these (24, 25, 29, 38, 44, 53, 62 and 66 in Table 2) are weak

according to theory. Note that in order for a feature to be confirmed and assigned as water we required its intensity to be  $> 10^{-23}$  cm/molecule and its frequency to be within  $0.001 \text{ cm}^{-1}$ . 40 of the 52 lines have been independently identified and assigned in the Sunspot spectra (Zobov et al. 2006). Of the 19 remaining lines not identified in BT2, 13 are also present in the sunspot spectra (Wallace et al. 1995) and 4 of these 13 have been in fact assigned to water (Zobov et al. 2006 and private communications). Many of the observed features are blends of multiple lines (often 2, the para:ortho pair lines): for these cases we assigned the band to the strongest component (ortho in the case of pairs of lines).

Figures 3 and 4 show examples of our line assignment with the observed stellar spectrum on the top panel overplotted to the sunspot spectrum (offset from the BS587 spectrum by +0.05), and with a synthetic water linelist computed at 3500 K on the bottom panel. Note that the choice of temperature for the synthetic water spectrum is *not* a best fit but was chosen to represent a bright cool stellar atmosphere and is close to that of the sunspot spectrum. In fact, a synthetic spectrum at 3000K may be more representative of a 3500K giant since the gas temperatures of the layers where most flux is emitted are typically 500K less than the effective temperature of the star (Allard et al. 1997). We have compared a 3000K synthetic water linelist with BS587 and find that the same number of water lines are identified.

Some of the lines identified as water transitions in the observed spectra are not from experimentally-known levels. For some of these cases the quantum numbers have not been fully determined and those given in Table 2 are the rigorous ones only from the ab initio data. We have singled out these transitions in italic in Table 2. Finally, it is worth noting that some of the identified lines are in fact ro-vibrational: we have excluded these transitions from our sensitivity analysis (see next section and Table 3).

### **3.1 Temperature sensitive water lines: a theoretical study**

Once the water lines have been assigned, we attempt to determine the sensitivity of each pure rotational transition to small (25 K) changes in temperature. This can be determined by simply estimating the *relative* intensity of the lines as a function of temperature by the use of modified Boltzmann equation:

$$I_{rel} \sim 10^{-15} \frac{g_{lower}}{U} \exp\left(-\frac{E_{lower}}{kT}\right)$$

where  $g_{lower}$  and  $E_{lower}$  are respectively the statistical weight and the energy level for the lower rotational state, and U is the total partition function (which is a function of the temperature, T).



Table 2. –continued

	Frequency (cm <sup>-1</sup> )	$\nu_1\nu_2\nu_3$ (u)	J (u)	$K_a K_c$ (u)	$\nu_1\nu_2\nu_3$ (l)	J (l)	$K_a K_c$ (l)	E(l)	Sunspot	$T_{max}$ (K)
57	894.542	010	19	7 13	010	18	4 14	6095.5140	Y	1500
58	894.637	000	20	8 13	000	19	5 14	5052.6689	Y	1500
59	894.697		29			28		19917.3223	N	4000
60	894.746	010	23	7 16	010	22	6 17	8181.3570	Y	1500
61	894.806	020	24	15 10	020	23	14 9	12832.5041	Y	2950
62	894.920	100	18	4 15	100	17	1 16	6885.4857	Y	1500
63	895.026								N	
64	895.070								Y	
65	895.094		22			21		15222.2697	N	3375
66	895.154	100	20	8 13	100	19	5 14	8618.8825	Y	1500
67	895.203	001	20	5 15	001	19	4 16	8286.0153	Y	1500
68	895.252	000	25	22 3	000	24	21 4	11756.8965	Y	2750
69	895.335								N	
70	895.376								N	
71	895.423 <sup>1</sup>	100	13	9 5	100	12	6 6	6051.2728	Y	3375

<sup>1</sup> assigned by Zobov et al. (private communications) in the sunspots.

Note that our choice of 25K is rather arbitrary: in order to use pure rotational water lines as good tools for the determination of the effective temperature of low mass stars, we require these lines to be sensitive to temperature changes below the temperature discrepancy found by other methods, usually at least 100K. We calculated the partition function using the fitting formula of Harris et al. (1998) (Equation 12) which is suitable for high temperatures. We have considered temperatures ranging from 1500 K to 4000 K in steps of 25 K. Examples of intensities and gradients versus temperature are given in Figure 5 for two pure rotational water transitions: while the weak water transition at 797.424 cm<sup>-1</sup> (line 5 from Table 2) exhibits a fairly low and flat gradient, the water transition at 894.637 cm<sup>-1</sup> (line 58 from Table 2) is very sensitive to temperature changes up to ~ 2800 K but it becomes less sensitive at higher temperatures. The temperature of the maximum gradient (i.e the temperature at which the transition is most sensitive to temperature changes) for all lines is also given in Table 2 (last column). We find that about 10 transitions out of the 36 pure rotational ones identified in the BT2 linelist are sensitive enough to small (25K) temperature changes that they could potentially be used in the determination of an effective temperature scale for low mass stars. Clearly, a 25K sensitivity is a strict requirement. A 50K sensitivity would still make our methodology more accurate than others and would lead to the use of a larger number of lines: from the 36 pure rotational ones identified here **we find about 14**.

The use of the most temperature sensitive water transitions for the determination of an accurate effective temperature scale of low mass stars becomes practical once a range of calibration objects has been observed with suitable measurements of water transitions. Our two dwarf stars only span around 300 K and have inadequate S/N for these purposes. Nevertheless, we attempt here to demonstrate the methodology by computing the intensity and gradient of the *pure rotational*

transitions from Table 2 at 3500K. Our computations are shown in Table 3 which includes the subset of rotational lines and identifiable in the Sunspot atlas. From this table we see that some of the most sensitive lines, at this particular temperature, are around  $894.6 \text{ cm}^{-1}$ . In Figure 6 we plot the ratio of the two stellar spectra for a small wavelength region centred at  $894.6 \text{ cm}^{-1}$  and compare it to the ratio of two synthetic spectra computed at 3200 and 3500K. The strength of the ‘absorption’ for some of the lines in the divided spectra is a clear indication that the transitions identified from Table 3 are indeed the most sensitive to temperature variations. It should be noted that the strongest most sensitive water lines occur towards lower temperatures. Observations of cooler objects should be within the reach of instruments such as EXES on SOFIA. The method can be calibrated with measurements of the growing number of cool low-mass eclipsing binaries.

Finally, an effective temperature scale for low mass stars can only be quantitatively derived if effects such as stellar rotation, internal **and atmospheric** structure and equation of state are taken into consideration when generating the synthetic spectra.

#### 4 CONCLUSIONS

In this paper we present the first high resolution MIR spectra of M dwarfs. Very high resolution observations of pure rotational water vapour transitions in the MIR may provide us with a new methodology in the determination of the effective temperatures for low mass stars. We have used the latest state-of-the-art water linelist (BT2, Barber et al. 2006) to identify and assign water transitions in these spectra. In total we assign 52 water lines out of 71 likely water transitions; 36 are pure rotational lines. We have computed a theoretical sensitivity study to determine how sensitive each pure rotational water transition is to small (25 K) changes in effective temperature and we find that at least 10 should be sensitive enough to be used as temperature indicators.

Due to the small wavelength region observed, the lack of a statistical sample of objects spanning lower temperatures and the low S/N, it is impossible at this stage to determine the effective temperature of our two M dwarfs using the methodology outlined in this work; our technique is viable only provided we have a large enough number of sensitive rotational lines (hence a larger number of wavelength regions in the 8-21  $\mu\text{m}$  spectrum), as well as a large sample of objects spanning the cool spectral subsequences. Both TEXES on Gemini and future generation telescopes such as the ELT have the potential to achieve this.

Beside the need of a larger sample of objects, ultimately, for a realistic determination of an



**Table 3.** Relative intensity of pure rotational and assigned water lines at 3500K (Column 3), and Gradient at 3500K (Column 4).

	Frequency (cm <sup>-1</sup> )	Intensity (3500K)	Gradient (3500K)
2	797.188	5.97E-21	9.48E-26
5	797.424	4.19E-22	3.24E-25
6	797.551	3.05E-21	6.36E-25
9	798.122	6.68E-21	1.08E-25
18	799.919	7.33E-22	4.51E-25
21	800.169	1.23E-21	5.75E-25
23	800.280	7.24E-21	2.86E-25
25	800.427	1.14E-21	5.58E-25
28	800.552	1.28E-21	5.84E-25
29	800.611	4.67E-22	3.47E-25
30	801.132	1.07E-21	5.43E-25
31	801.159	6.08E-22	4.06E-25
32	801.219	5.56E-21	2.02E-25
33	801.252	5.98E-21	9.27E-26
34	801.360	3.46E-21	5.98E-25
39	892.199	1.43E-21	6.08E-25
40	892.228	3.78E-22	3.03E-25
41	892.286	1.63E-21	6.32E-25
42	892.345	6.58E-21	8.00E-26
44	892.578	2.13E-22	2.05E-25
45	892.634	3.96E-22	3.12E-25
46	892.724	3.52E-22	2.89E-25
47	892.760	2.14E-22	2.06E-25
48	892.805	1.10E-21	5.49E-25
49	892.838	3.05E-22	2.63E-25
51	892.891	1.39E-21	8.59E-26
52	893.937	1.81E-21	6.48E-25
54	894.214	1.28E-21	5.85E-25
57	894.542	1.27E-20	2.55E-24
58	894.637	1.95E-20	6.34E-24
60	894.746	5.38E-21	2.47E-25
61	894.806	2.61E-21	4.71E-25
62	894.920	9.17E-21	9.86E-25
66	895.154	4.50E-21	4.38E-25
67	895.203	5.16E-21	3.00E-25
68	895.252	1.24E-21	5.77E-25

effective temperature scale, model atmospheres including the BT2 water linelist should be used for future analysis.

## 5 ACKNOWLEDGEMENTS

Based on observations obtained at the Gemini Observatory, which is operated by the Association of Universities for Research in Astronomy, Inc., under a cooperative agreement with the NSF on behalf of the Gemini partnership: the National Science Foundation (United States), the Science and Technology Facilities Council (United Kingdom), the National Research Council (Canada), CONICYT (Chile), the Australian Research Council (Australia), CNPq (Brazil) and SECYT (Argentina). Observations with TEXES (GN-2006B-Q-49) were supported by NSF grant AST-0607312. SV acknowledges financial support from an individual PPARC Advanced Fellowship. MJR acknowledges NSF grant AST-0708074. We thank the referee for constructive comments which helped to improve the manuscript.

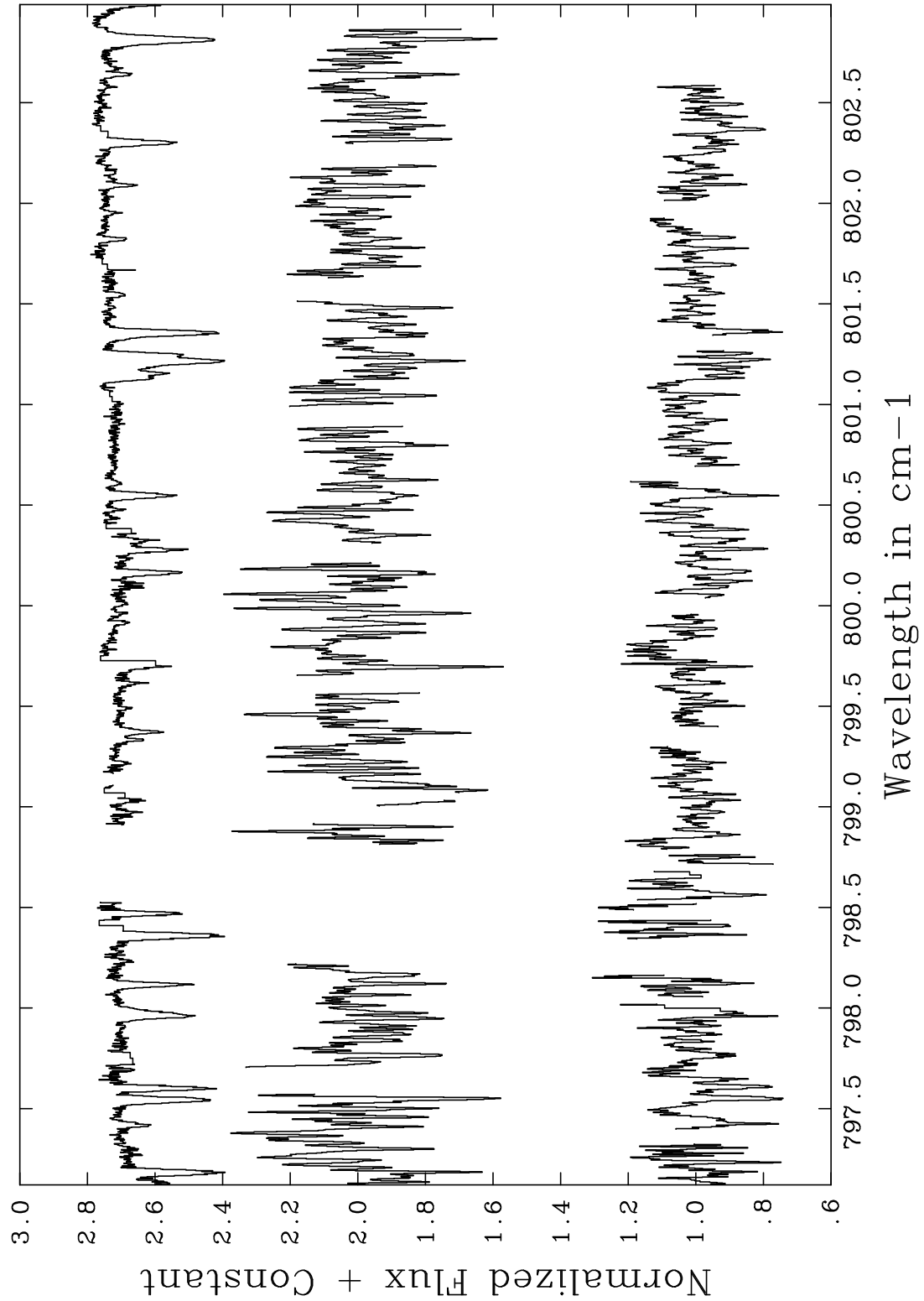


**Figure 1.** Observed spectra centred at  $11.2 \mu\text{m}$ . Top: BS587; Middle: GJ273; Bottom: GJ411. Spectra have been corrected for stellar velocities (see text).

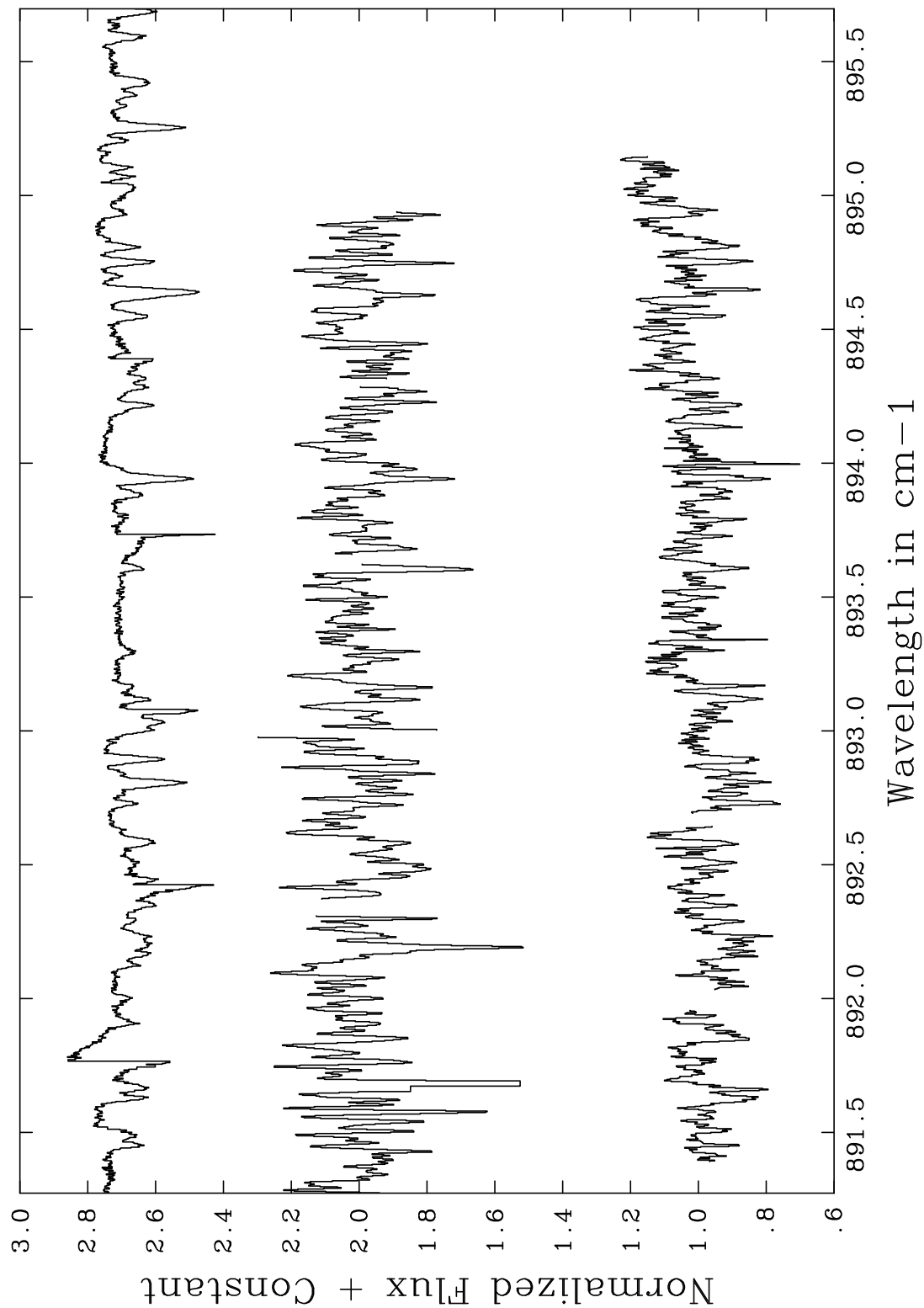
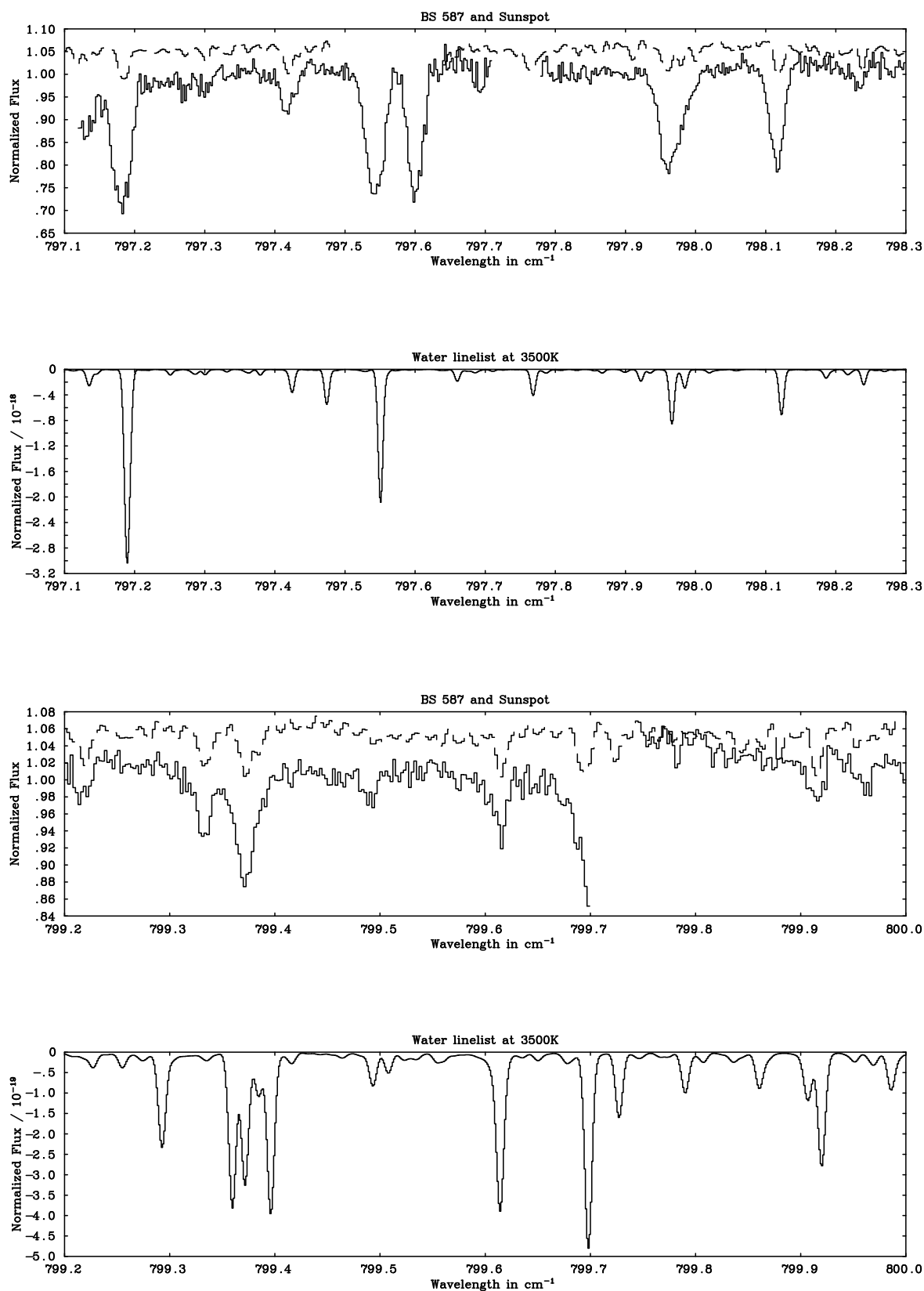


Figure 2. As for figure 1 for the 12.5  $\mu\text{m}$  region



**Figure 3.** Selected portions of spectra in the  $11.2 \mu\text{m}$  region. Top: BS587 (Continuous) overplotted to the Sunspot spectrum (dashed, flux offset by  $+0.05$  for clarity); Bottom: synthetic BT2 linelist computed at  $3500\text{K}$ .

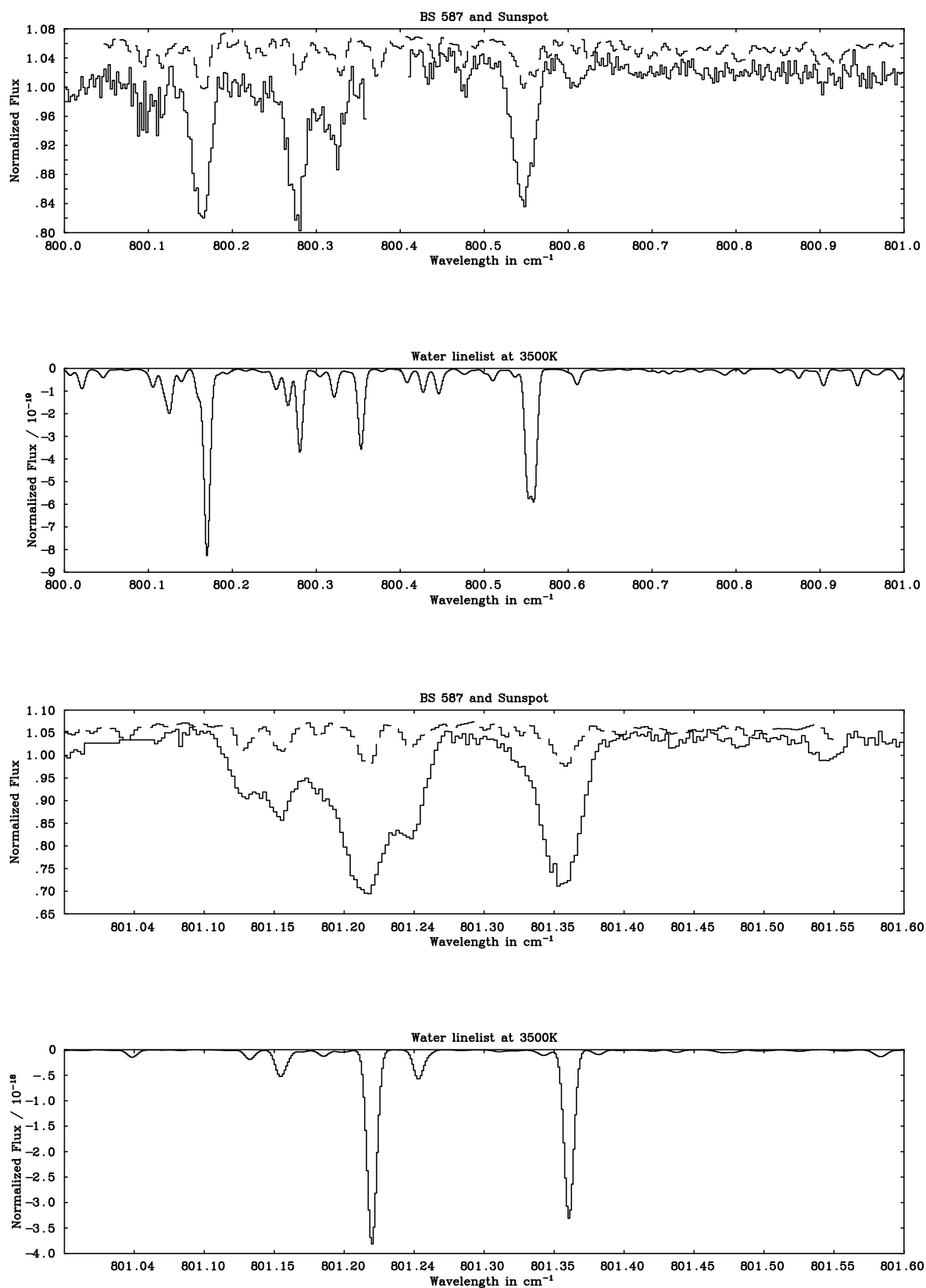
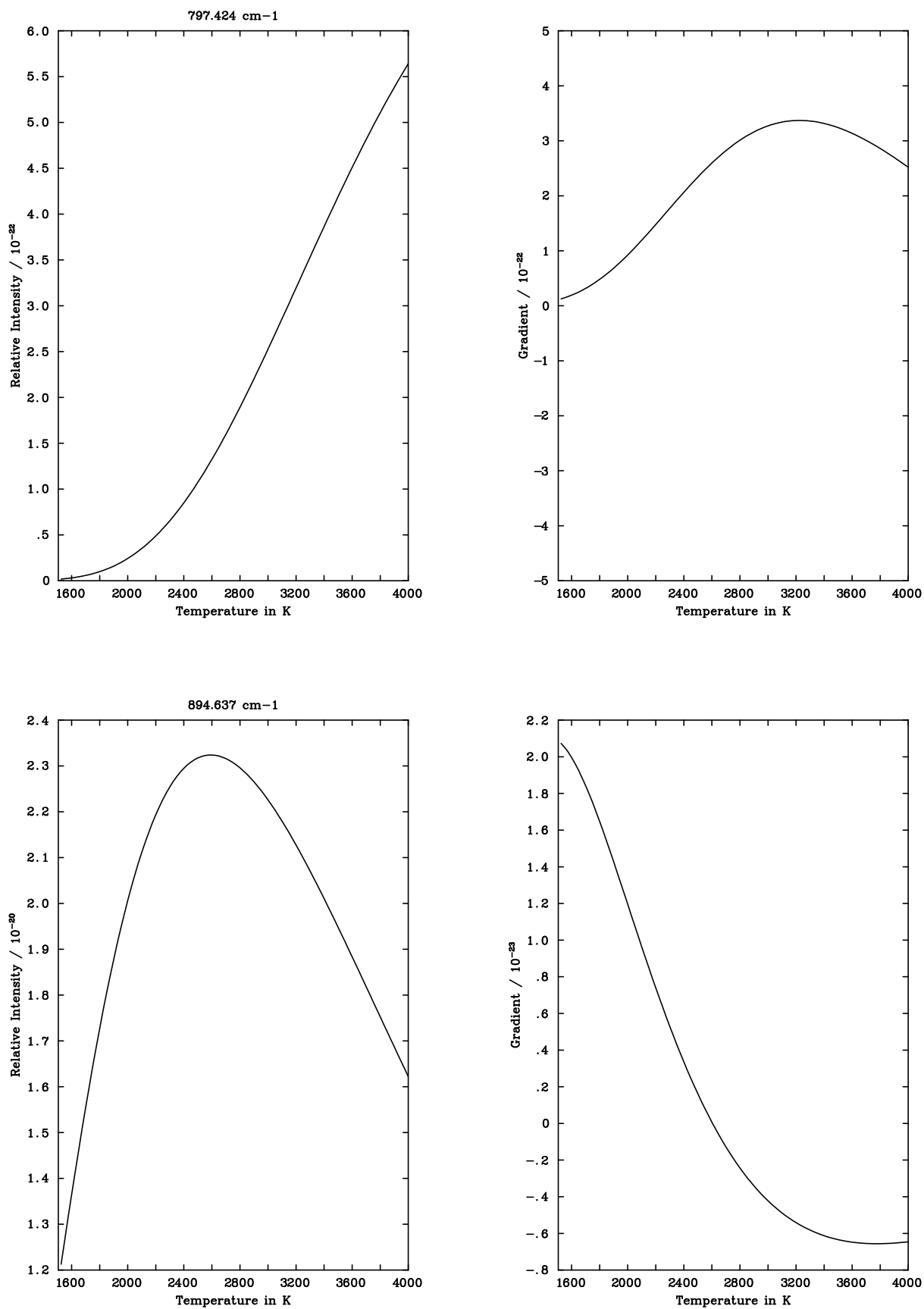
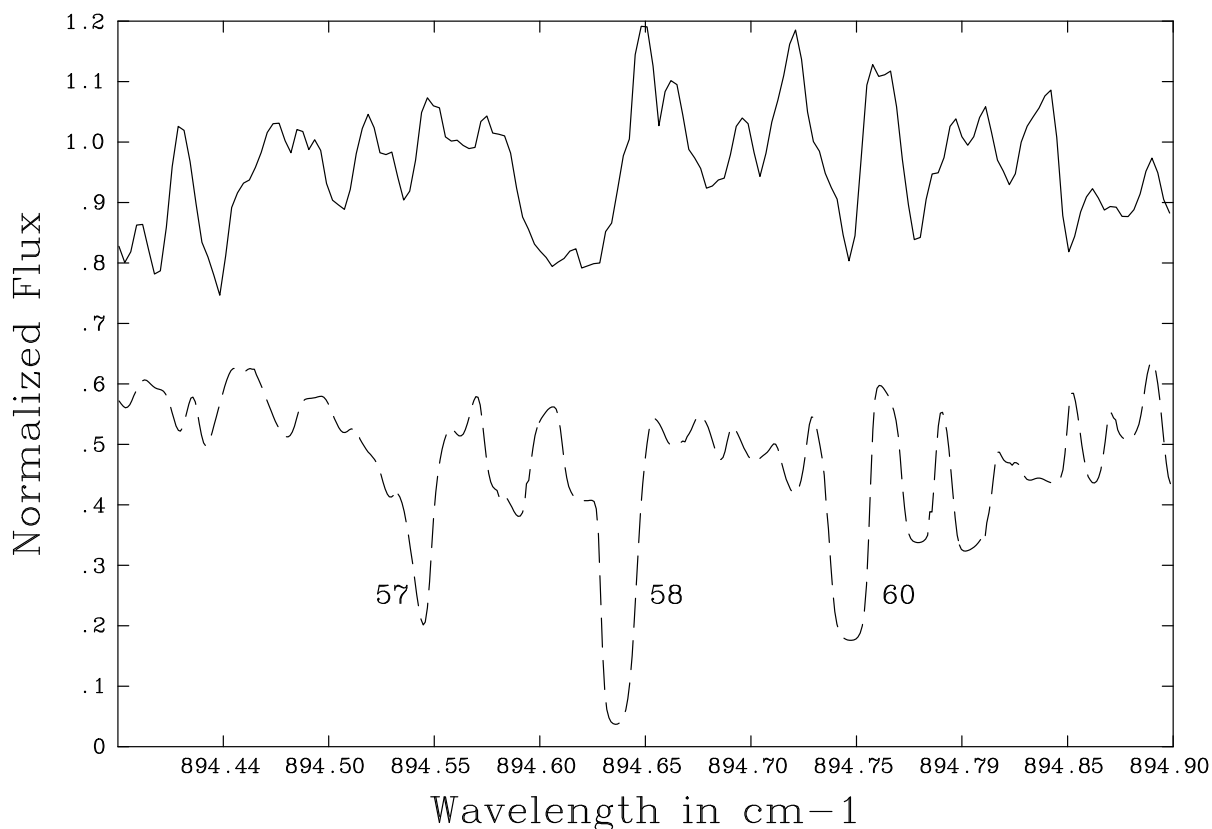


Figure 4. As in Figure 3 but for the 12.5 μm region



**Figure 5.** Relative Intensity (e.g. Column 2 in Table 2) versus temperature (Left) and actual gradient versus temperature (Right) for a weak (Top) and a strong (Bottom) pure rotational water transitions from Table 3. The top gradient has been multiplied by a factor of  $10^3$  to fit within the same scale as the bottom one.



**Figure 6.** Ratio of the GJ273 and GJ411 spectra (Top) compared to a ratio of two synthetic spectra computed using the BT2 water linelist, at 3200 and 3500K.

## REFERENCES

- Allard F., Hauschildt P. H., Schwenke D., 2000, *ApJ*, 540, 1005
- Allard F., Hauschildt P. H., Alexander, D. R., Starrfield, S., 1997, *ARA&A*, 35, 137
- Barber R. J., Tennyson J., Harris G. J., Tolchenov R. N., 2006, *MNRAS*, 368, 1087
- Coheur P.-F., Bernath P. F., Carleer M., Colin R., Polyansky O. L., Zobov N. F., Shirin S. V., Barber R. J. Tennyson J., *J. Chem. Phys.*, 2005, 122, 74307
- Cushing M. C., Rayner J. T., Vacca W. D., 2005, *ApJ*, 623, 1115
- Delfosse X., Forveille T., Perrier C., Mayor M., 1998, *A&A*, 331, 581
- Fluks M. A., Plez B., The P. S., de Winter D., Westerlund B. E., Steenman H. C., 1994, *A&AS*, 105, 311
- Harris G. J., Viti S., Mussa H. J., Tennyson J., 1998, *J. Chem. Phys.*, 109, 7197
- Hauschildt P. H., Baron E., Allard F., 1997, *ApJ*, 483, 390
- Kirkpatrick J. D., Kelly D. M., Rieke G. H., Liebert J., Allard F., Wehrse R., 1993, *ApJ*, 402, 643
- Jones H. R. A., Longmore A. J., Jameson R. F., Mountain C. M., 1994, *MNRAS*, 267, 413

- Jones H. R. A., Longmore A. J., Allard F., Hauschildt P. H., 1996, *MNRAS* 280, 77
- Jones H. R. A., Pavlenko Y., Viti S., Tennyson J., 2002, *MNRAS*, 330, 675
- Jones H. R. A., Pavlenko Y., Viti S., Barber R. J., Yakovina L. A., Pinfield D., Tennyson J., 2005, *MNRAS*, 358, 105
- Lacy J. H., Richter M. J., Greathouse T. K., Jaffe D. T., Zhu Q., 2002, *PASP*, 114, 153
- Leggett S. K., Allard F., Dahn C., Hauschildt P. H., Kerr T. H., Rayner J., 2000, *ApJ*, 535, 965
- Leggett S. K., Allard F., Geballe T. R., Hauschildt P. H., Schweitzer A., 2001, *ApJ*, 548, 908
- Marcy G.W., Lindsay V., Wilson K., 1987, *PASP*, 99, 490
- Partridge H., & Schwenke D. W., 1997, *J. Chem. Phys.*, 106, 4618
- Polyansky O. L., Zobov N. F., Viti S., Tennyson J., Bernath P. F., Wallace L., 1997a, *Science*, 277, 346
- Polyansky O. L., Zobov N. F., Viti S., Tennyson J., Bernath P. F., Wallace L., 1997b, *ApJL*, 489, 205
- Ryde N., Richter M. J., Harper G. M., Eriksson K., Lambert D. L., 2006, *ApJ*, 645, 652
- Tsuji T., Ohnaka K., Aoki, W, 1996, *A&A*, 305L, 1
- Zobov N. F., Shirin S. V., Polyansky O. L., et al., 2006, *J. Molec. Spectrosc.*, 237, 115
- Wallace L., Bernath P., Livingston W., Hinkle K., Busler J., Guo B., Zhang K., 1995, *Science*, 268, 1155